JOURNAL OF PETROLEUM GEOMECHANICS
(JPG)

Original article

The effect of the number, dimensions and location of anomalies on the crosswell Traveltime tomography results

Saeed Aftab[1]*, Rasoul Hamidzadeh Moghadam[1], Ahsan Leisi[1]

1- Faculty of Mining Engineering, Sahand University of Technology, Tabriz, Iran

Received: 2 February 2023; Accepted: 26 May 2023

DOI: 10.22107/JPG.2023.384315.1187

Keywords

2D Seismic Tomography, Crosswell Seismic Tomography, Simulation Crosswell Seismic Tomography, PyGIMLi , Seismic Analysis

Abstract

Seismic tomography is one of the seismic imaging techniques which are interesting due to the possibility of recording high-frequency seismic waves and providing the possibility of obtaining high-quality images from inside the earth. The ability to record high-frequency waves enables the identification of faults, fractures, and joints with sufficient accuracy, which are very important in reservoir geomechanics studies. In this paper 2D crosswell seismic tomography is simulated by PyGIMLi (python geophysical inversion and modeling library). Crosswell seismic tomography is a routine part of seismic explorations, particularly hydrocarbon exploration. Fast marching and Gauss-Newton methods are the default algorithms for Traveltime forward modeling and inversion, respectively. The fast marching method is a very efficient method for calculating the travel time and path of seismic waves in homogeneous and especially non-homogeneous environments. This method uses the finite difference algorithm to solve the eikonal equation in gridded velocity environments. The Gauss-Newton method is a powerful classic method that can work with all types of geophysical data, which by properly weighting the data and creating a constraint, makes the inversion process faster and more accurate So that the inversion error is below 5% in all cases. The results obtained from the inversion show that the Gauss-Newton method has performed well and the anomalies designed in the models have been correctly detected so that the results can be interpreted without difficulty. Also, changing survey parameters influenced the results of inversion and it was necessary to determine these parameters correctly so that the results of inversion are more accurate and precise. Simulation crosswell seismic tomography is an important step before a successful practical crosswell seismic tomography. In general, simulation before any geophysical survey can be very helpful.

1. Introduction

Recognition of the subsurface elastic characteristics from Crosswell Traveltime data is an essential and routine part of seismic explorations [1,2,3]. Standard and well-known methods for collecting seismic data involve deploying sources on or below the earth's surface for recording refracted, reflected, or diffracted back energy to receivers. Simulation before a practical process is necessary, which makes essential optimizations before a field survey. Geophysical surveys also need simulations. The simulation of seismic surveys makes the distances of the used geophones, the location of the drilling of exploratory wells, and the distances of the wells from each other to be optimally selected, and the amount of error in the data collection process is reduced. And in general, it can be concluded whether the desired method can be used for the intended purposes or not. One of the significant limitations of these techniques is that overburden and near-surface layers attenuate high-frequency waves that are essential for distinguishing subsurface structures with high resolution. Crosswell Traveltime tomography is a way to circumvent this limitation. In this method, both energy sources and receivers are put in cross wells so the high-frequency signals can be recorded and

* **Corresponding Author:** Gmail address: saeedaftab1996marand@gmail.com, PO. BOX 51335/1996

high-resolution images from the earth's interior can be extracted [4,5,6,7,8]. Due to its similarity to medical X-ray tomography, which visualizes the human body interior, the seismic ray approach is terming seismic-ray tomography. But the problems of seismic-ray tomography are different from X-ray tomography to render straight-line methods inadequate specifically when the survey region involves high-velocity inhomogeneities that are appealing for geophysics experts. The first difference is in experimental geometry. For geophysical surveys the sources and receivers can scarcely place on all sides of the study region, so, in some subregions, the ray coverage is inadequate. Significantly in the perpendicularly oriented structures to ray paths that are well covered, however, these regions may have rays with a limited range of angles and result in poor resolution. The second significant difference is in physics; the X-ray tomography for medical applications, X-rays travel along straight lines while for seismic applications, the elastic waves are severely distorted by strongly inhomogeneous media [1]. The seismic tomography approach applies to many subsurface investigations such as hydrocarbon reservoir monitoring [9], underground water surveying [10], and ore body delineating [11]. Traveltime tomography consists of three main steps: picking the observed seismic Traveltime, seismic wave ray tracing kinematically, and inversion of Traveltime for medium characterization [1]. Different strategies using for well source-receiver geometry [4], but this paper is concerned with the case where sources and receivers have deployed in wells and the seismic signal has transmitted from the source which is located in one well, to a receiver array in a neighboring well (**Fig. 1**). The resulting data are processing to create a reflection image or to map the acoustic velocity or other properties (velocity of P - and S waves, for example) of the area between wells.

In the last years, geophysicists have successfully used seismic tomography to image velocity variations of the earth's interior. In so doing, combined analysis of the P- and S wave information provides an efficient basis for the petrologic interpretation and lithologic classification [12]. We can estimate the porosity and permeability from P-wave velocity [13]. Velocity information has been used for the estimation of saturation, mineralogy, and other essential applications [14,15,16,17].

This paper is not focused on the applications of velocity for petrophysical estimations. However, we focused on the 2D Traveltime forward modeling and Traveltime inversion to obtain the P-wave velocity. To study the efficiency of seismic tomography for estimating the P-wave velocity, we considered synthetic models. In these models, we also studied the effect of the sensor spacing (sensor numbers) and well spacing on the inversion results. The term seismic tomography refers to all seismic methods that can produce images from inside the Earth. But in previous studies, crosswell seismic tomography has rarely been done, rather reflection and refraction methods have been used. In addition, there is no specific software and rule for forward modeling and inversion in crosswell seismic tomography. The methods introduced in this article can be considered as a rule. The written codes can be added to industrial software or introduced as independent code or software. Also, we tried to simulate the actual conditions of seismic tomography as much as possible. Things such as the existence of noise, the ray path effect, the seismic wave distortion, and the way of covering seismic waves should be included in the advanced modeling so that the physical understanding of this problem becomes more tangible.

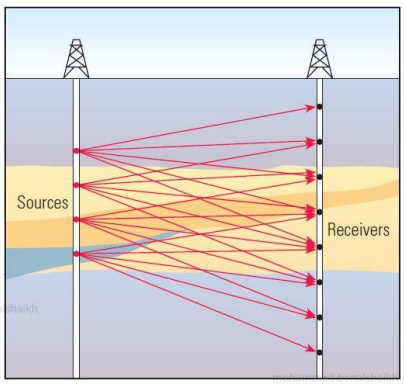

Fig. 1. Schematic figure for crosswell seismic tomography.

2. Methodolgy

2.1. Forward modeling with fast marching method (FMM)

One of the significant problems in exploration seismology is robustly and accurately predicting seismic ray Traveltime and the path of seismic energy between two points within a laterally heterogeneous 2D or 3D medium [18,19,20]. A

more recently developed and very prominent class of method, particularly in the exploration industry, for predicting seismic ray Traveltime in complex media is to seek finite-difference (FD) solutions to the eikonal equation throughout a gridded velocity field. The main disadvantage of FD eikonal solvers is that they often suffer from stability problems; in particular, the progressive integration of Traveltimes along an expanding square, which is commonly used to calculate the Traveltime field, has the potential to breach causality in the presence of large velocity gradients. The basic of the FMM method is briefly described below; for more details, refer to Sethian, (1996) [21]; Sethian, (1999) [22]; Rawlinson and Sambridge, (2005) [18]. The eikonal equation, which governs the propagation of seismic waves, may be written as:

$$|\nabla_x T| = s(x) \quad (1)$$

Where ∇_x is the gradient operator, T is Traveltime, and $s(x)$ is slowness (vice versa of velocity) as a function of position x. A considerable problem for FD methods that seek to solve the eikonal equation for the first-arrival Traveltime field is that the wavefront may be discontinuous in gradient. This problem occurs when the wave front self-intersects (multi-pathing) but later-arriving information discarded. After the calculation Traveltime, the main purpose is inverting Traveltime to achieve P-wave velocity, therefore the generalized Gauss-Newton method is used for data inversion [18].

2.1. Gauss-Newton inversion

The default inversion framework in PyGIMLi is based on the generalized Gauss-Newton method that is compatible with any given forward modeling operator and thus applicable for different geophysical problems, which is a significant advantage for the Gauss-Newton inversion method [23]. We state the inversion problem as the minimization of an objective function consisting of data misfit and model constraints:

$$\|W_d(Am - d)\|_2^2 + \lambda\|W_m(m - m_0)\|_2^2 \rightarrow \min \quad (2)$$

Where W_d is data weighting matrix containing the inverse data errors, W_m is the model constraint matrix (for example first-order roughness matrix), m_0 is a reference model, m is the model parameters vector, d is the data vector, A is the forward modeling operator, or kernel, and λ is the dimensionless factor that scales the influence of the regularization term. Note that we use transformations to restrict parameters to reasonable ranges, and we do not include inequality constraints in minimization. There is a various regularization method (mixed operators, damping factor, different kind of smoothness). The application of the Gauss-Newton scheme on minimizing Equation 3 yields the model update Δm^k in the k^{th} iteration [23].

$$\left(J^T W_d^T W_d J + \lambda W_m^T W_m\right)\Delta m^k = J^T W_d^T W_d(\Delta d^k) - \lambda W_m^T W_m(m^k - m_0) \quad (3)$$

$$\Delta d^k = d - Am^k \quad (4)$$

$$\Delta m^k = m^k - m^{k-1} \quad (5)$$

Which is solved using a conjugate-gradient least-squares solver. In Equation 3, J is the Jacobian matrix. The inversion process is sketched in **Fig. 2**. Here we used PyGIMLi (Python Geophysical Inversion and Modeling Library) in both forward modeling and inversion. PyGIMLi has been in active development since 2009 and covers diverse needs research and education in geophysics. the Python programming language was selected as the basis for PyGIMLi for its flexible, free of cost, and cross-platform-compatible nature, which makes it widely used in geoscience [23,24,25,26,27,28,29,30].

The basic geophysical tasks to solve with PyGIMLi are modeling and inversion. For the Traveltime forward modeling, the fast-marching method (FMM) uses. FMM is a finite-difference (FD) solution of the eikonal equation. Like most other grid-based techniques, FMM is only capable of locating the first-arrival phase in continuous media; however, its combination of rapid calculation and unconditional stability makes it a practical scheme for velocity fields of arbitrary complexity. We used the generalized Gauss-Newton approach with flexible regularization, which is the default inversion method in PyGIMLi, and we used this method for inversion.

3. Results and discussion

Here we considered synthetic geological models to test the efficiency of seismic tomography for the reconstruction of the earth's interior structure. Also, we studied the effect of the senor spacing and wells spacing on inversion results.

3.1. Two blocks model with different

velocities in homogenous media

The first synthetic model consists of two blocks and homogenous media. The first block in the upper part of the section is a low-velocity zone and the second block in the lower part of the synthetic section is a high-velocity block. The reference model and inversion result are represented in **Fig. 3**. As shown in **Fig. 3**, both blocks in the inversion result, are correctly reconstructed, that correct and accurate detection of the anomalies is essential. According to the inversion result, the Gauss-Newton method is efficient for the detection of mass anomalies. Note how the rays are attracted by the high-velocity anomaly block while circumventing the low-velocity region. The attraction of seismic rays reflected in seismic ray coverage in **Fig. 4**. Another important point about the seismic rays' distortion from straight lines, this phenomenon happens when the seismic rays enter the zones with different velocities, so the seismic rays' direction changes, and given in **Fig. 4**.

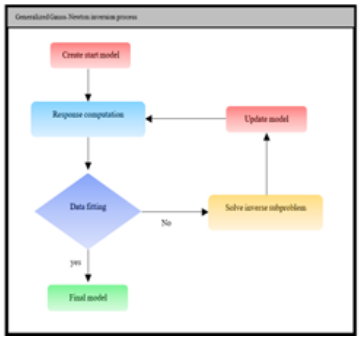

Fig. 2. Generalized Gauss-Newton scheme.

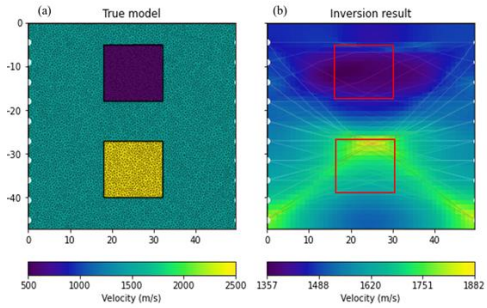

Fig. 3. The reference model shown in part a, and the inversion result with Gauss-Newton method shown in part b.

Another array of blocks is when the low-velocity block is near the left well and the high-velocity block is near the right one. The reference model and inversion result for this array are shown in **Fig. 5** and the seismic rays coverage is shown in **Fig. 6**, and the position of the blocks has marked with red boxes. The area in **Fig. 5**, marked by the yellow box, may be interpreted as an anomaly, but the low velocity of this area is created due to the ray path effect of the inversion process and has nothing to do with the anomaly. Also, we tested the juxtaposition blocks array and the reference model, and the inversion result of this array is shown in **Fig. 7**, and seismic rays coverage is shown in **Fig. 8**. For the juxtaposition blocks array, it is difficult to interpret the inversion result as juxtaposition blocks and means that the vicinity of individual zones with different velocities harms the inversion result and disrupts interpretation. In the last two arrays, the characteristics of the seismic tomography survey were not altered, and just the position of the blocks changed.

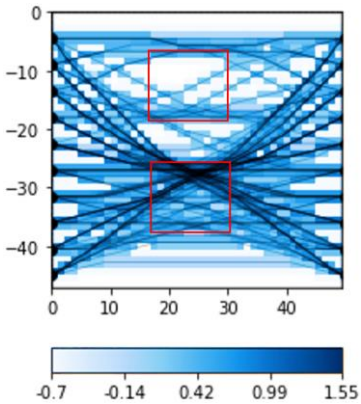

Fig. 4. The transmitted seismic ray path in the first synthetic model. It is obvious that the density of the rays in the high-velocity block is more than the low-velocity block.

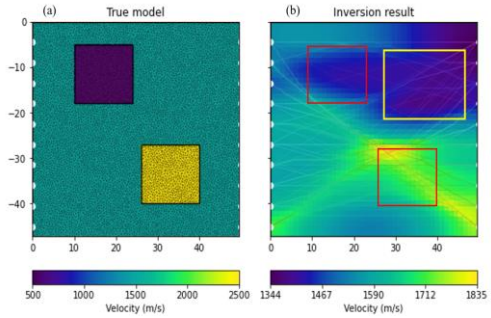

Fig. 5. The two-block reference model where the blocks are placed in cross-section corners part a, and the inversion results for this model part b. The low velocity zone, which is marked by a yellow box shows the ray path effect.

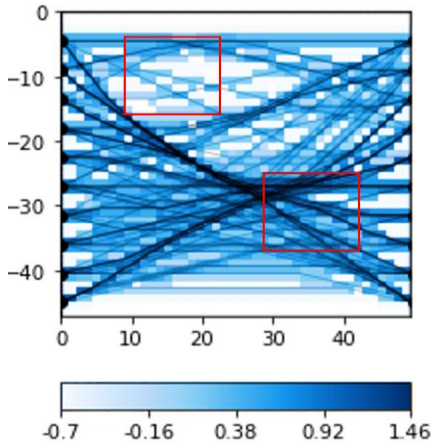

Fig. 6. The seismic ray coverage for the two-block. synthetic model where the blocks are placed in cross-section corners. The density of the rays in the high-velocity block is more than the low-velocity block.

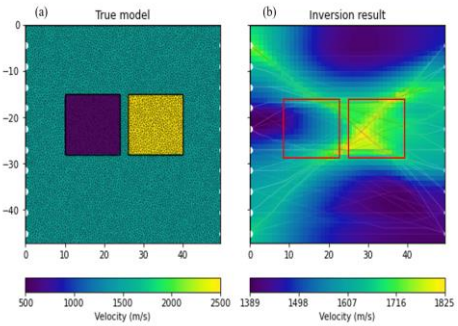

Fig. 7. The first synthetic model with juxtaposition blocks array is shown in part a. The inversion result for this array shown in part b, and position of the blocks with red boxes.

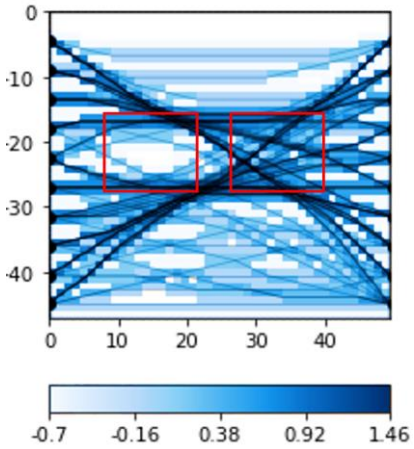

Fig. 8. The seismic ray coverage for the first synthetic model with juxtaposition blocks array and the red boxes shows the position of the blocks.

Note that the position of the blocks in all three arrays in inversion results does not represent the actual position of the blocks, they moved a bit and must be considered in the interpretations. The Existence of noise is usual in geophysics-measured data. Therefore, we added 10 microseconds of absolute noise.

The number of iterations for all three arrays and Chi-squared values is represented in **Fig. 9**. In **Fig. 9**, the red curve is related to blocks placed below each other (first array in **Fig. 3**, part a), the blue curve is related to blocks that positioned in the section corners (second array in **Fig. 5**, part a), and the green curve represent the juxtaposition blocks (third array in **Fig. 7**, part a). For the first iterations, the Chi-squared value is high, but with increasing iterations and optimization of inversion result, the Chi-squared value decreases to reach a constant rate.

Note that, due to different climatic conditions, the appropriate arrangement method should be chosen according to that climate, and one type of survey is not the answer in all situations.

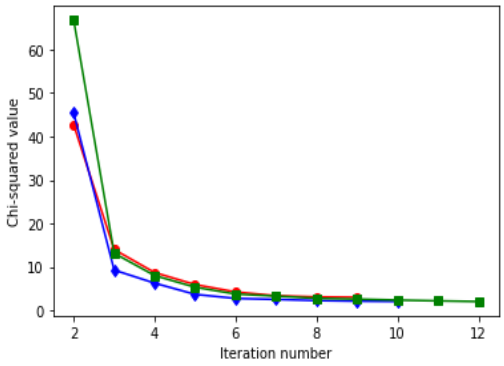

Fig. 9. The number of iterations for Gauss-Newton inversion process and relation of the Chi-squared values with iteration numbers. Red curve related to the first array when the blocks positioned below each other, the blue curve related to blocks that position.

3.2. synthetic lens model

The fourth model for testing seismic tomography is the lens model, in which anomaly bodies are distributed in different parts of the section. The reference model and inversion result are in **Fig. 10**. The anomaly bodies in this model had reconstructed correctly, and we can interpret the inversion result as a lens model. The seismic ray's coverage is in **Fig. 11**. The ray's density in different parts of the section well represents the location of the anomaly bodies. The tomography

survey specification for this model, like the previous cases and dimensions of the anomaly bodies are varied. In this case, the velocity of all anomaly bodies same, but we also tested the seismic tomography for the lens model with the different velocities of anomaly bodies. The inversion result is not accpetable for this case, and only one of the anomaly bodies is distinctly recognizable. The reference model and inversion result are in **Fig. 12**. The seismic ray's coverage is in **Fig. 13**, and the anomaly positions are marked. The Chi-squared values for the lens models (lens models with the constant and different velocities of the anomaly bodies) are in **Fig. 14**.

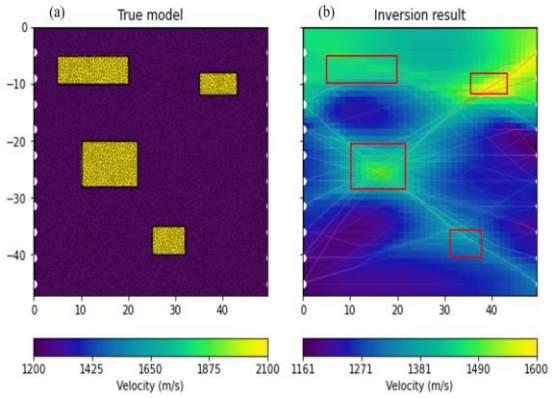

Fig. 10. (a) true synthetic lens model and (b) inversion result and red boxes represent the position of the anomaly bodies.

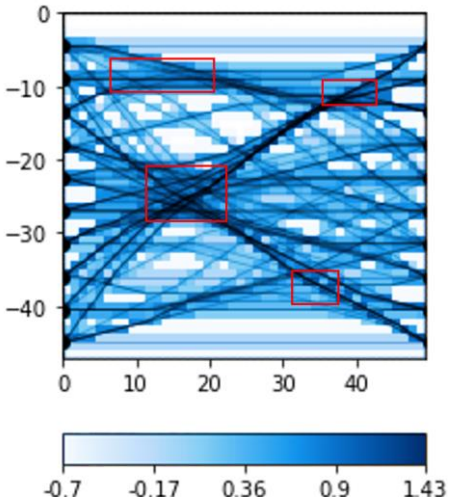

Fig. 11. Seismic ray's coverage for the synthetic lens model. Position of the anomaly bodies represented by red boxes.

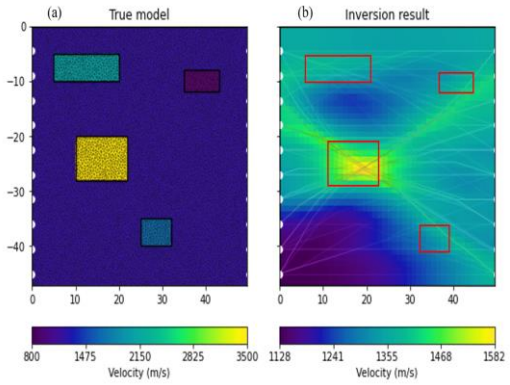

Fig. 12. (a) the true lens model with different velocity of the anomaly bodies and (b) is inversion result for this case. The red boxes represented the position of the anomaly bodies.

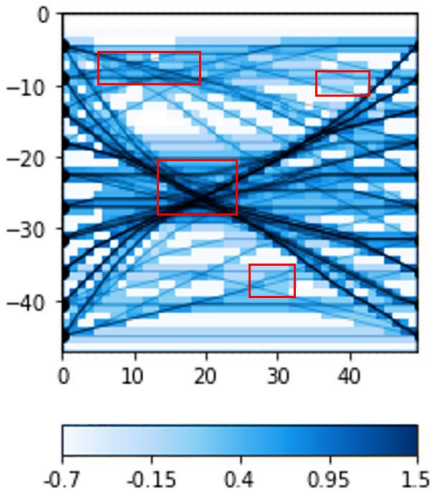

Fig. 13. The seismic ray's coverage for the lens model with different velocity of anomalies and position of the anomalies represented by red boxes.

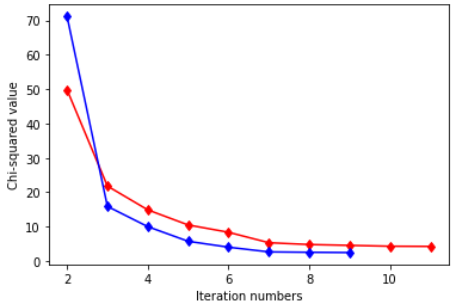

Fig. 14. The Chi-squared values for the lens model. The red and blue curves are related to the lens model with constant velocity and different velocities of anomaly bodies respectively.

4. Conclusion

We found that the seismic survey simulation and appropriate selection of survey parameters is the first and most essential step for geophysical studies and interpretations. Note that in cases where the geology of the study area is complex, the performance of the crosswell seismic tomography method will not necessarily be ideal. The interpretation of the results of inversion in this method is not unique and may be interpreted in different ways. The ray path effect of seismic waves makes the interpretation of the inversion results more difficult and in some cases may cause a lot of errors in the interpretation procedure. Correcting the ray path effect can improve the inversion results. Improvement of the forward modeling method to justify the movement of seismic waves can affect the software development of seismic modeling methods. Seismic simulations and seismic surveys can be very effective for geomechanical studies and subsurface interpretations. We hope that we and other researchers will be able to use seismic simulations in the oil, mining, and water industry soon.

5. References

[1] Zhou, B., Greenhalgh, S., Green, A., 2008, nonlinear Traveltime inversion scheme for cross hole seismic tomography in tilted transversely isotropic media: Geophysics, **73**(4), 17–33. https://doi.org/10.1190/1.2910827

[2] Ajo-Franklin, J. B., Peter, J., Doetsch, J., Daley, T. M., 2013, High-resolution characterization of a CO2 plume using crosswell seismic tomography: Cranfield, MS, USA: International Journal of Greenhouse Gas Control, 18, 497–509. http://dx.doi.org/10.1016/j.ijggc.2012.12.018

[3] Onishi, K., Ueyama, T., Matsuoka, T., Dai Nobuoka, D., Saito, H., Azuma, H., Xue, Z., 2009, Application of crosswell seismic tomography using difference analysis with data normalization to monitor CO2 flooding in an aquifer: international journal of greenhouse gas control, 3, 31 1 – 32 1. doi:10.1016/j.ijggc.2008.08.003

[4] Bregman, N. D., Bailey, R. C., Chapman, C. H., 1988, Cross hole seismic tomography: Geophysics, **54**(2), 200-215. https://doi.org/10.1190/1.1442644

[5] Mao, S., Lecointre, A., Hilst, R. D., Campillo, M., 2022, Space-time monitoring of groundwater fluctuations with passive seismic interferometry: nature communications. https://doi.org/10.1038/s41467-022-32194-3

[6] Barone1, I., Cassiani1, G., Ourabah, A., Boaga, J., Pavoni1, M., Deiana, R., 2022, Surface wave tomography using dense 3D data around the Scrovegni Chapel in Padua, Italy: Scientific Reports. https://doi.org/10.1038/s41598-022-16061-1

[7] Hanafy, S. H., Hoteit, H., Li, J., Schuster, G. T., 2021, Near-surface real-time seismic imaging using parsimonious interferometry: Scientific Reports. https://doi.org/10.1038/s41598-021-86531-5

[8] Bianco, M. J., Gerstoft, P., Olsen, K. B., Lin, F. C., 2019, High-resolution seismic tomography of Long Beach, CA using machine learning: Scientific Reports. https://doi.org/10.1038/s41598-019-50381-z

[9] Lee, D. S., Stevenson, V. M., Johnston, P. F., Mullen, C. F., 1995, time-lapse crosswell seismic tomography to characterize flow structure in the reservoir during the thermal stimulation: Geophysics, **60**(3), 660-665. https://doi.org/10.1190/1.1443805

[10] Zelt, C. Z., Azaria, A., Levander. A., 2006, 3D seismic refraction Traveltime tomography at a groundwater contamination site: Geophysics, **71**(5), 67–78. https://doi.org/10.1190/1.2258094

[11] Malehmir, A., Tryggvason, A., Wijns, C., Koivisto, E., Lindqvist, T., 2018, why 3D seismic data are an asset for exploration and mine planning? Velocity tomography of weakness zones in the Kevitsa Ni-Cu-PGE mine, northern Finland: Geophysics, **83**(2), 33–46. https://doi.org/10.1190/geo2017-0225.1

[12] Bauer, K., Schulze, A., Ryberg, T., Sobolev, S. V., Weber, M. H., 2003, Classification of lithology from seismic tomography: A case study from the Messum igneous complex, Namibia: Journal of Geophysical Research, **108**(9), 1-15. https://doi.org/10.1029/2001JB001073

[13] Parra, J. O., Hackert, C. L., 2006, Permeability and porosity images based on P-wave surface seismic data: Application to a south Florida aquifer: Journal of Geophysical Research, **42**(2415), 1-14. https://doi.org/10.1029/2005WR004114

[14] Leisi, A., Falahat, R., 2021, Investigation of Some Porosity Estimation Methods Using Seismic Data in One of the South Iranian Oil Fields: Journal of Petroleum Research, 31(119), 22–25. (in persian). https://doi.org/10.22078/pr.2021.4438.3007

[15] Leisi, A., Kheirollahi, H., Shadmanaman, N., 2022, Investigation and comparison of conventional methods for estimating shear wave velocity from well logging data in one of the

sandstone reservoirs in southern Iran: Iran. J. Geophys. (in persian). https://doi.org/https://doi.org/10.30499/IJG.2022.320098.1385

[16] Kheirollahi, H., Shad Manaman, N., Leisi, A., 2023, Robust estimation of shear wave velocity in a carbonate oil reservoir from conventional well logging data using machine learning algorithms: Journal of Applied Geophysics, 211, 104971. https://doi.org/10.1016/j.jappgeo.2023.104971

[17] Leisi, A., Saberi, M. R., 2022, Petrophysical parameters estimation of a reservoir using integration of wells and seismic data: a sandstone case study: Earth Science Informatics. https://doi.org/10.1007/s12145-022-00902-8

[18] Rawlinson, N., Sambridge, M., 2005, The Fast Marching Method: An Effective Tool for Tomographic Imaging and Tracking Multiple Phases in Complex Layered Media: Exploration Geophysics, **36**(4), 341-350. https://doi.org/10.1071/EG05341

[19] Ronczka, M., Hellman, K., Günther, T., Wisén, R., Dahlin, D., 2017, Electric resistivity and seismic refraction tomography: a challenging joint underwater survey at Äspö Hard Rock Laboratory: Solid Earth, 13, 671-682. https://doi.org/10.5194/se-8-671-2017

[20] Heincke, H., Günther, T., Dalsegg, E., Rønning, J. S., Ganerød, G. V., Elvebakk. H., 2010, combined three-dimensional electric and seismic tomography study on the Åknes rockslide in western Norway: Journal of Applied Geophysics, **70**(4), 292-306. https://doi.org/10.1016/j.jappgeo.2009.12.004

[21] Sethian, J. A., 1996, a fast marching level set method for monotonically advancing fronts: Proceedings of the National Academy of Science, **93**(4), 1591-1595. https://doi.org/10.1073/pnas.93.4.1591

[22] Sethian, J. A., 1999, Level Set Methods and Fast Marching Methods, New York, Cambridge University of press.

[23] Rückera, C., Güntherb, T., Wagner, F. M., 2017, PyGIMLi : An open-source library for modelling and inversion in geophysics: Computers and Geosciences, 109, 106-123. https://doi.org/10.1016/j.cageo.2017.07.011

[24] Schaa, R., Gross, L., du Plessis, J., 2016, PDE-based geophysical modelling using finite elements: examples from 3D resistivity and 2D magnetotellurics: Journal of Geophysics and Engineering, **13**(2), S59–S73. https://doi.org/10.1088/1742-2132/13/2/S59

[25] Cockett, B., Kang, S., Heagy, L. J., Pidlisecky, A., Oldenburga. D. W., 2015, SimPEG: An open source framework for simulation and gradient based parameter estimation in geophysical applications: Computers and Geosciences, 85, 142-154. https://doi.org/10.1016/j.cageo.2015.09.015

[26] Weigand, M., Kemna, A., 2016, Debye decomposition of time-lapse spectral induced polarisation data: Computers and Geosciences, 86, 34-45. https://doi.org/10.1016/j.cageo.2015.09.021

[27] Guyer, J. E., Wheeler, D., Warren, J. A., 2009, FiPy: Partial Differential Equations with Python: Computing in Science and Engineering, **11**(3), 6-15.

[28] Wellmann, J. F., Croucher, A., Regenauer-Lieb, K., 2012, Python scripting libraries for subsurface fluid and heat flow simulations with TOUGH2 and SHEMAT: Computers and Geosciences, 43, 197-206. https://doi.org/10.1016/j.cageo.2011.10.011

[29] Pérez, F., Granger, B. E., Hunter, J. D., 2011, Python: An Ecosystem for Scientific Computing: Computing in Science and Engineering, **13**(2), 13-21.

[30] Hector, H., Hinderer, J., 2016, pyGrav, a Python-based program for handling and processing relative gravity data: Computers and Geosciences, 91, 90-97. https://doi.org/10.1016/j.cageo.2016.03.010